Supplemental Information to "Two-phase fluid flow properties of cataclastic fault rocks: Implications for CO_2 storage in saline aquifers"

Here we present: (i) The relative permeability and capillary pressure curves used in the simulations; (ii) details of the properties of the Mam Tor siltstone that was used as analogue data to supplement the brine relative permeability measurements obtained from the fault rock samples; (iii) further output from the simulation models.

Relative permeability and capillary pressure curves used

The host rock relative permeability and capillary pressure curves (Fig. DR1, solid lines) were derived from laboratory measurements of undeformed samples of Permian Yellow Sands, using the procedures outlined in the main text. For the "two-phase case" simulation models, upscaled relative permeability functions (Fig. DR1A, dashed lines) are used for the cells adjacent to the fault in the hanging-wall compartment to govern the phase-specific flow across the fault. These curves are derived using an analytical solution, as a function of the host rock and fault rock absolute permeability, porosity, relative permeability and capillary pressure, as well as the fluid viscosities and densities, fault rock thickness, the host rock cell size, the across-fault flow rate and whether the across-fault flow represents a drainage or imbibition process. In this case the across-fault flow rate used ($1.2x10^{-8}$ m/s) is deduced from the "single-phase case" simulation results, and a drainage process is used in the upscaling since the non-wetting fluid (CO_2) is replacing the water in the fault. Capillary pressure is not upscaled since unlike relative permeability it cannot be a directional property, and capillary pressure effects are included in the upscaled relative permeability functions. Comprehensive details of the upscaling procedures are given in Manzocchi et al. (2008).

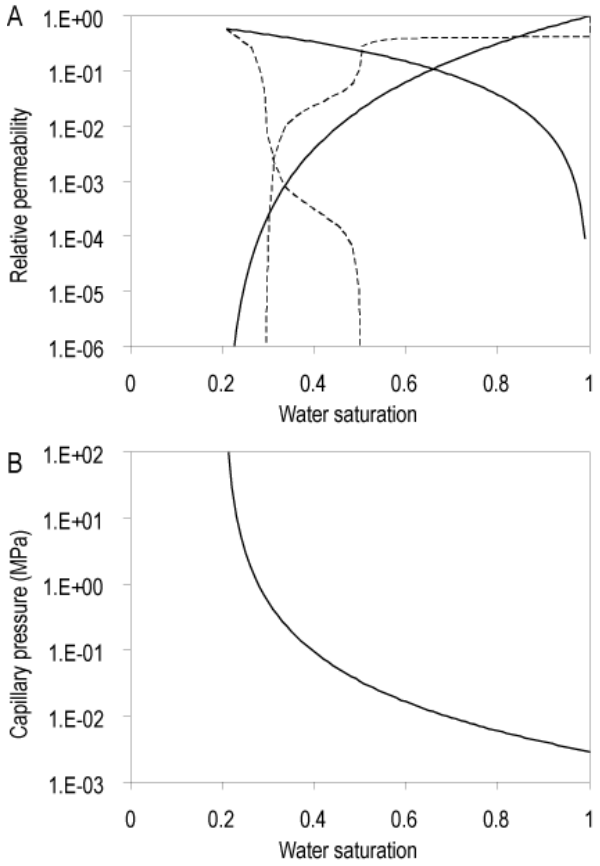

Figure DR1. Gas and water relative permeability versus water saturation (A) and capillary pressure versus water saturation (B) curves used as model input. Solid lines: Host rock curves. Dashed lines: Upscaled fault rock curves. The host rock capillary pressure curve shown was converted from a laboratory gas/water system to a system of supercritical CO_2 and brine under subsurface conditions as described in the main text.

Mam Tor data

To supplement fault rock brine relative permeability data we used results obtained from an analogue sample. The sample used is a low porosity (4%) and permeability (0.002 mD) siltstone obtained from Mam Tor, Derbyshire, UK (N53^o, 20’ 54”; W 1^o 48’ 3”). The siltstone is a distal turbidite of Namurian age (Allen, 1960). A BSEM image of the sample is shown in Fig. DR2.

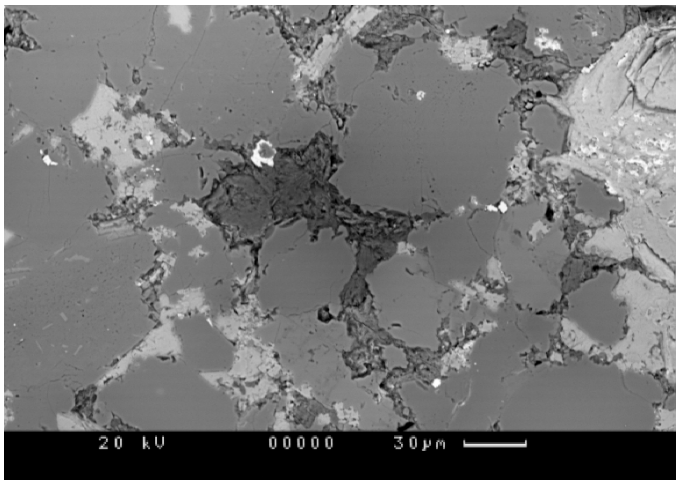

Figure DR2. BSEM image of the Mam Tor sample.

Additional results from simulation models

Fig. DR3 to DR6 show the CO_2 saturation at various times (5, 10, 25 and 50 years) after the start of injection. Fig. DR7 and DR8 show data on the brine and CO_2 relative permeabilities in the gridblocks immediately upstream and downstream of the fault. An important point to gain from these figures is that the CO_2 relative permeability in the upstream cell is far lower when no fault is present than in either the single- or two-phase case (Fig. DR7C). This is because the fault allows a higher capillary pressure to occur, which increases the CO_2 saturation and CO_2 relative permeability compared to the case when no fault is present. These results explain why pressure increases for the single-phase model are quite similar to those in the model without the fault. On the other hand, in the cells immediately downstream of the fault (Fig. DR8), the lowest CO_2 relative permeability is for the two-phase case because the fault acts as a flow baffle and consequently CO_2 saturations are low.

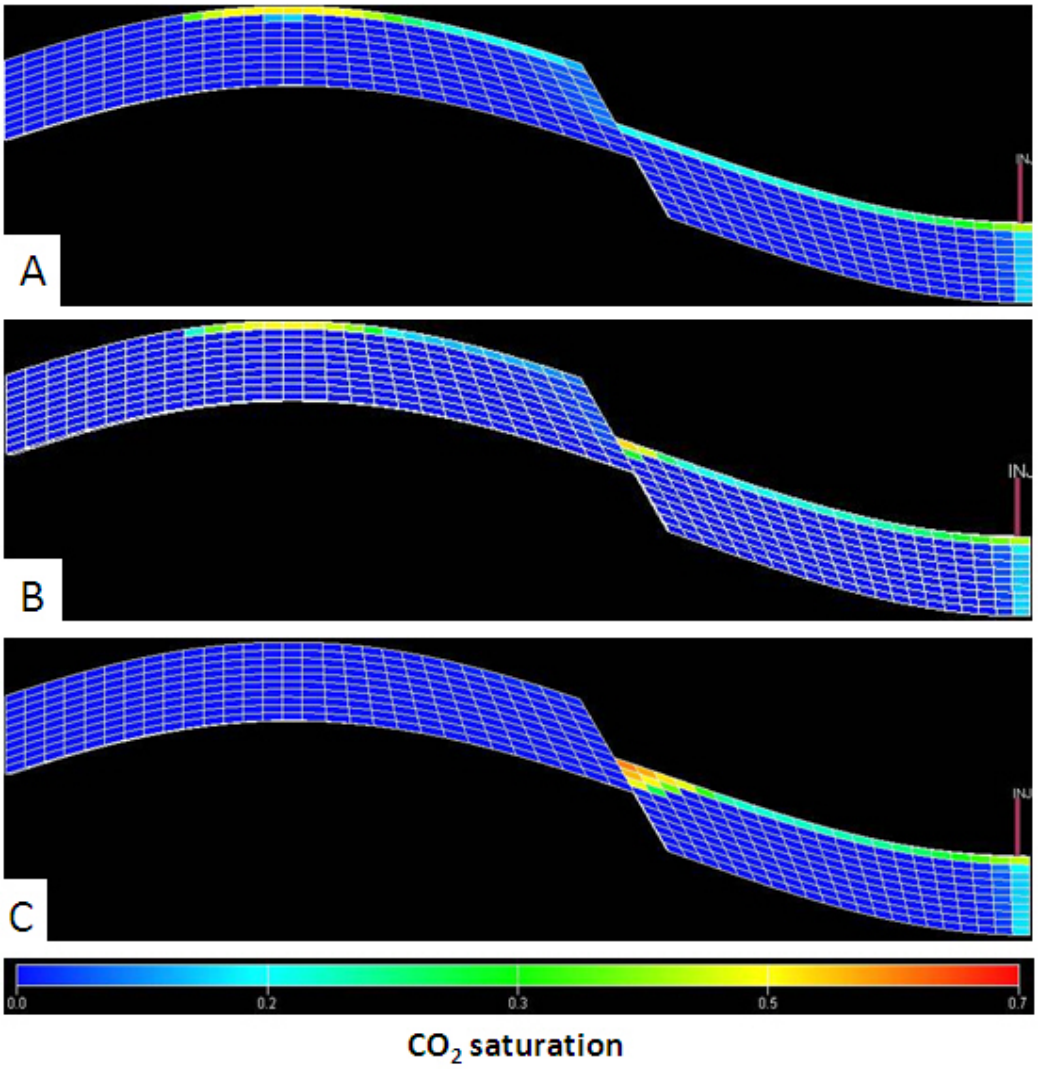

Figure DR3. CO_2 saturation in the central cross-section of the three models after 5 years of CO_2 injection. A) Host case. B) Single-phase case. C) Two-phase case.

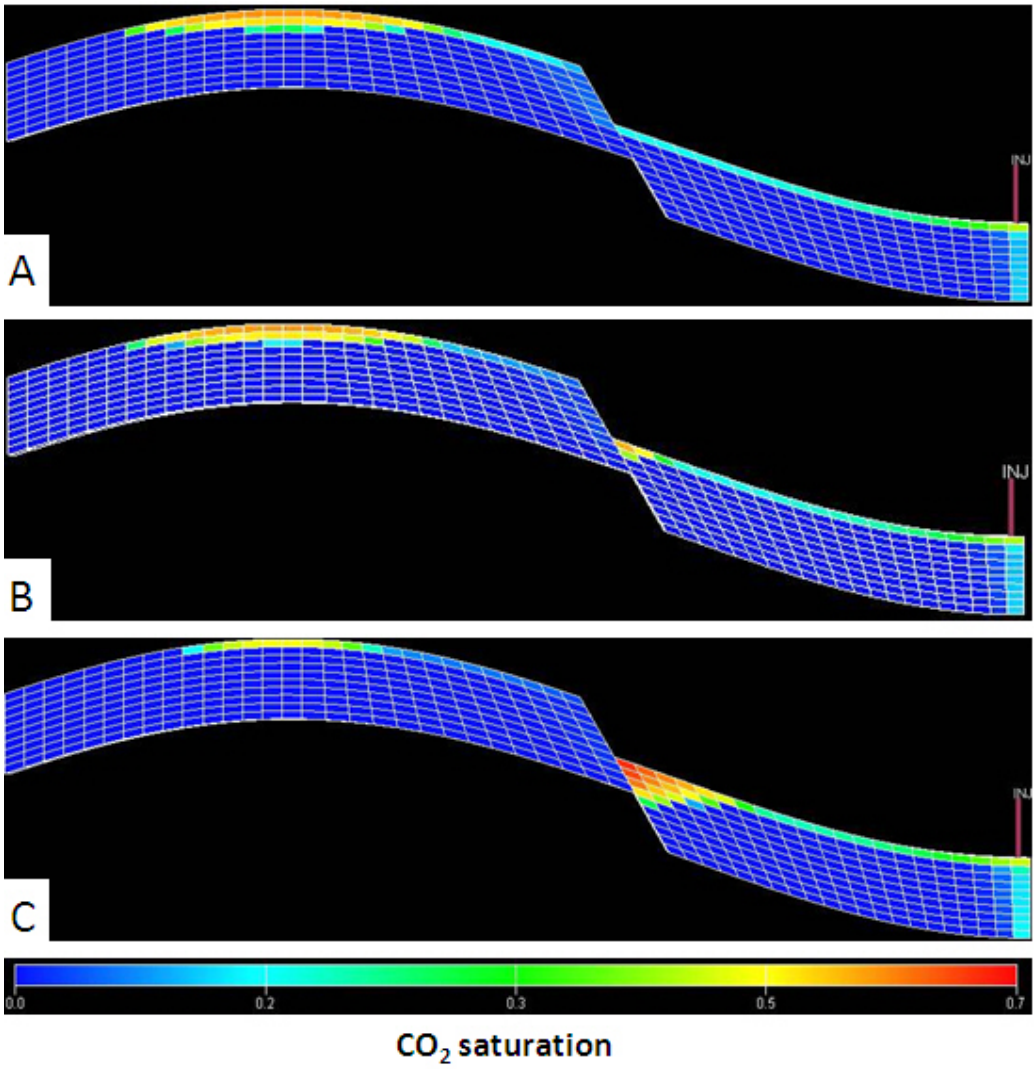

Figure DR4. CO_2 saturation in the central cross-section of the three models after 15 years of CO_2 injection. A) Host case. B) Single-phase case. C) Two-phase case.

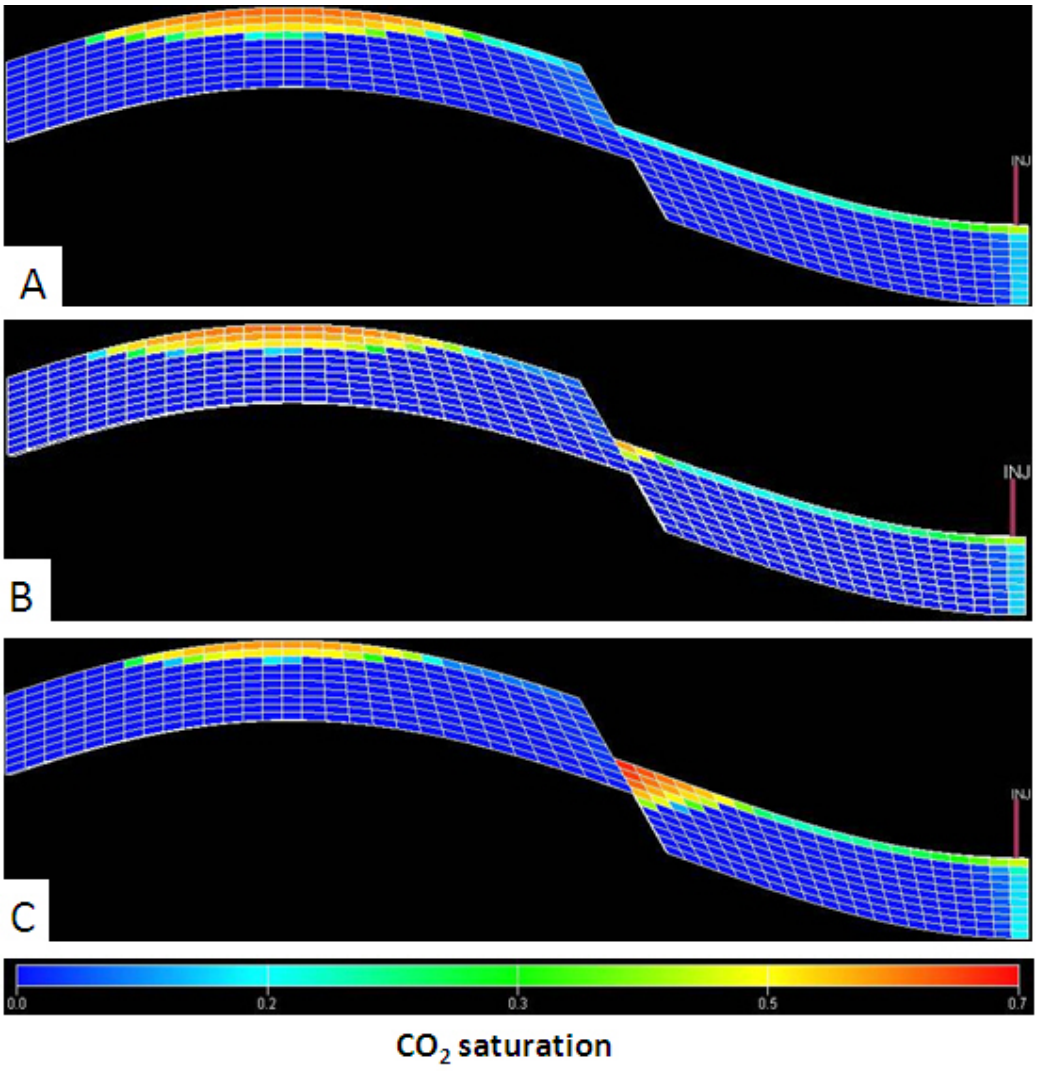

Figure DR5. CO_2 saturation in the central cross-section of the three models after 25 years of CO_2 injection. A) Host case. B) Single-phase case. C) Two-phase case.

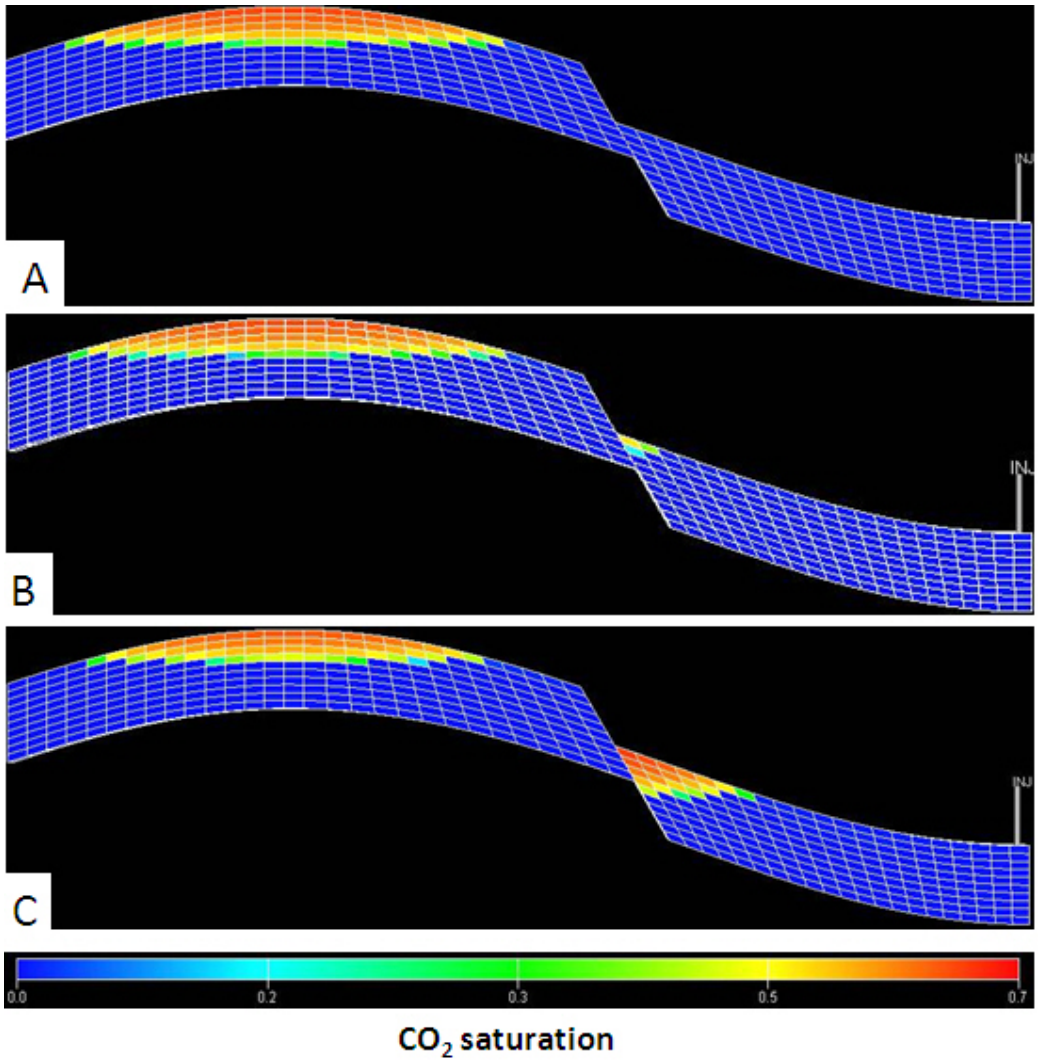

Figure DR6. CO_2 saturation in the central cross-section of the three models 50 years from the start of CO_2 injection (i.e. 10 years after the CO_2 injection has finished). A) Host case. B) Single-phase case. C) Two-phase case.

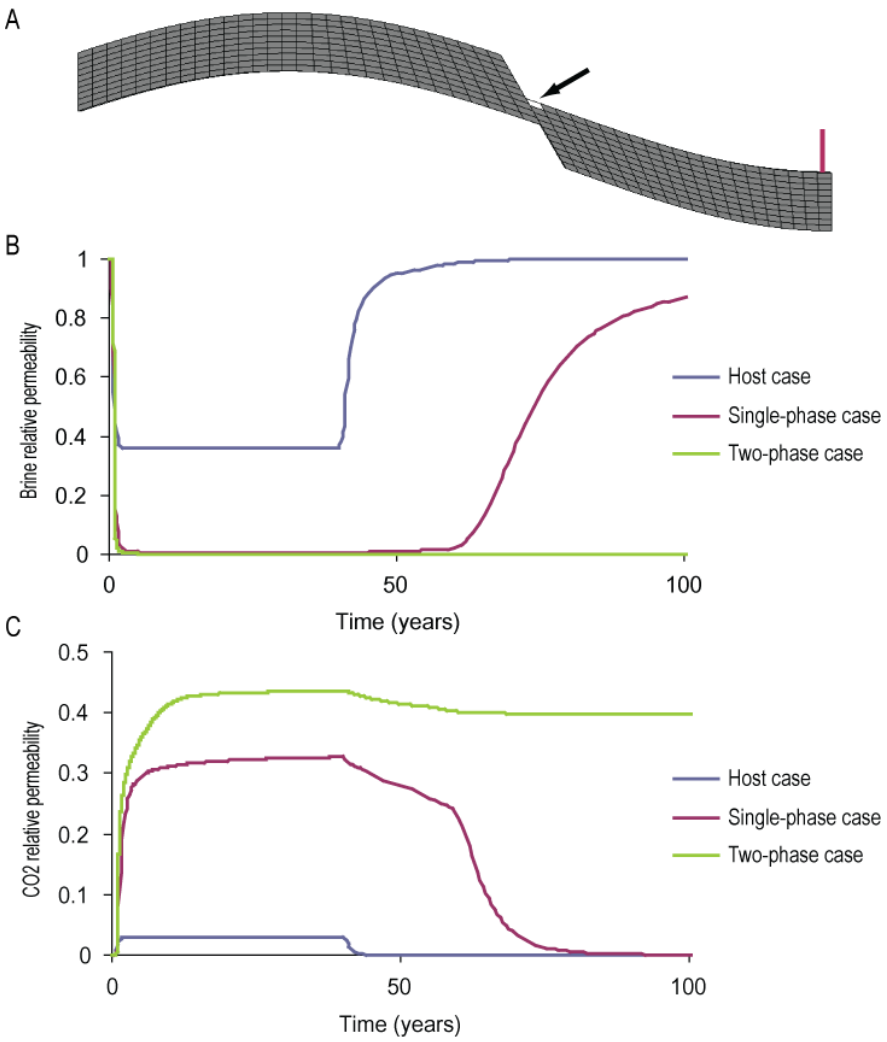

Figure DR7. Results from simulation models in the grid cell upstream (A) of the fault. Included are: B) Brine relative permeability; and C) CO_2 relative permeability.

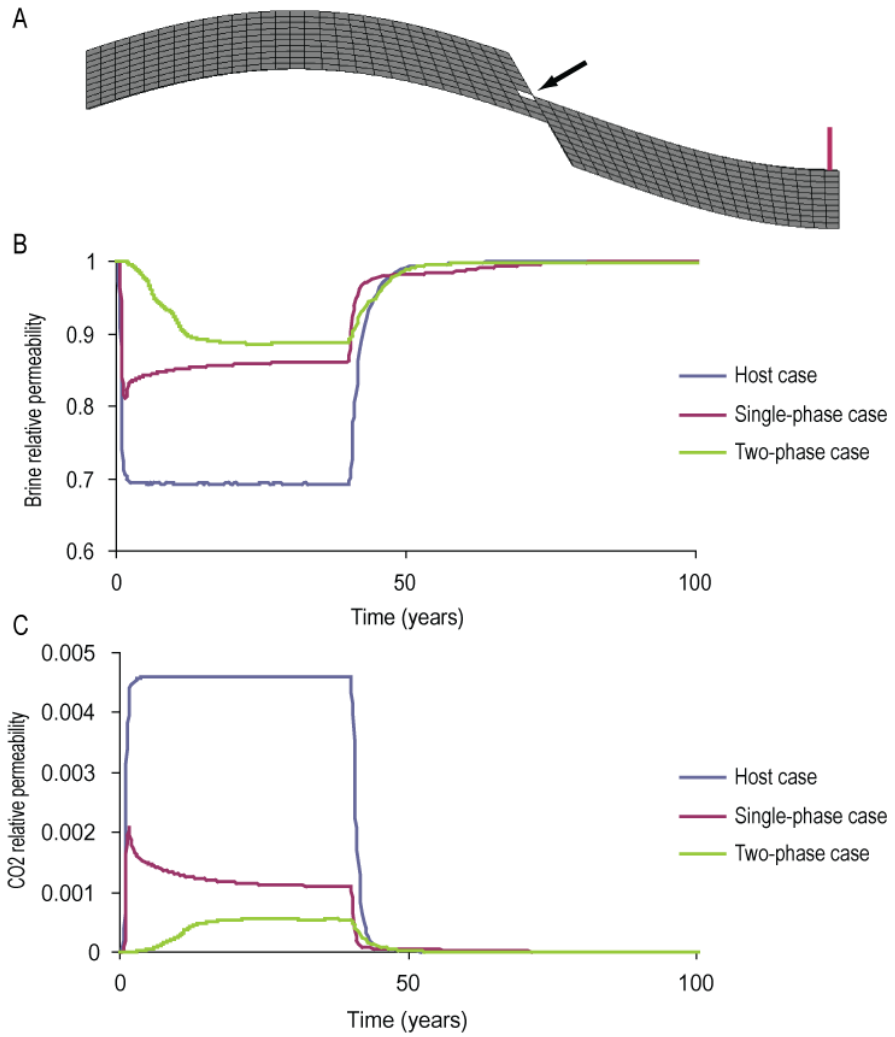

Figure DR8. Results from simulation models in the grid cell downstream (A) of the fault. Included are: B) Brine relative permeability; and C) CO_2 relative permeability.

REFERENCES CITED

Allen, J.R.L., 1960, The Mam Tor sandstones, a "turbidite" facies of the Namurian deltas of Derbyshire, England: Journal of Sedimentary Research, v. 30, p. 193–208.

Manzocchi, T., Heath, A.E., Palananthakumar, B., Childs, C., and Walsh, J.J., 2008, Faults in conventional flow simulation models: A consideration of representational assumptions and geological uncertainties: Petroleum Geoscience, v. 14, p. 91–110.